THE ANATOMICAL RECORD PART A 283A:288–299 (2005)

Modeling Masticatory Muscle Force in Finite Element Analysis: Sensitivity Analysis Using Principal Coordinates Analysis

CALLUM F. ROSS,[1]* BIREN A. PATEL,[2] DENNIS E. SLICE,[3] DAVID S. STRAIT,[4] PAUL C. DECHOW,[5] BRIAN G. RICHMOND,[6] AND MARK A. SPENCER[7]

[1]Organismal Biology and Anatomy, University of Chicago, Chicago, Illinois
[2]Interdepartmental Doctoral Program in Anthropological Sciences, Stony Brook University, Stony Brook, New York
[3]Institute for Anthropology, University of Vienna, Vienna, Austria
[4]Department of Anthropology, University at Albany, New York
[5]Baylor College of Dentistry, Texas A&M Health Science Center, Dallas, Texas
[6]Department of Anthropology, Center for the Advanced Study of Hominid Paleobiology, George Washington University, Washington, District of Columbia,
[7]Department of Anthropology, Institute for Human Origins, University of Arizona, Tempe, Arizona

ABSTRACT

Our work on a finite element model of the skull of *Macaca* aims to investigate the functional significance of specific features of primate skulls and to determine to which of the input variables (elastic properties, muscle forces) the model behavior is most sensitive. Estimates of muscle forces acting on the model are derived from estimates of physiological cross-sectional areas (PCSAs) of the jaw muscles scaled by relative electromyographic (EMG) amplitudes recorded in vivo. In this study, the behavior of the model was measured under different assumptions regarding the PCSAs of the jaw muscles and the latency between EMG activity in those muscles and the resulting force production. Thirty-six different loading regimes were applied to the model using four different PCSA sets and nine different PCSA scaling parameters. The four PCSA sets were derived from three different macaque species and one genus average, and the scaling parameters were either EMGs from 10, 20, 30, 40, 50 and 60 msec prior to peak bite force, or simply 100%, 50%, or 25% of peak muscle force. Principal coordinates analysis was used to compare the deformations of the model produced by the 36 loading regimes. Strain data from selected sites on the model were also compared with in vivo bone strain data. The results revealed that when varying the external muscle forces within these boundaries, the majority of the variation in model behavior is attributable to variation in the overall magnitude rather than the relative amount of muscle force generated by each muscle. Once this magnitude-related variation in model deformation was accounted for, significant variation was attributable to differences in relative muscle recruitment between working and balancing sides. Strain orientations at selected sites showed little variation across loading experiments compared with variation documented in vivo. These data suggest that in order to create an accurate and valid finite element model of the behavior of the primate skull at a particular instant during feeding, it is important to include estimates of the relative recruitment levels of the masticatory muscles. However, a lot can be learned about patterns of skull deformation, in fossil species for example, by applying external forces proportional to the estimated relative PCSAs of the jaw adductors.

Key words: electromyography; muscle force; mastication; primates; principal coordinates analysis; finite element analysis

Our work on a finite-element model (FEM) of the macaque monkey skull has two principal aims. The first is to build an accurate FEM validated by in vivo bone strain data. Once this task is completed, we will investigate the effects on the model of altering model geometry and external forces, thereby addressing hypotheses regarding the functional significance of changing skull form and function during primate ontogeny and evolution. For example, what is the effect of reducing the size of the browridges, removing the postorbital septum, or repositioning the palate rostrally or caudally relative to the braincase?

The second aim of our work is to determine whether FEMs of fossil primate skulls, such as that of *Australo-*

*Correspondence to: Callum F. Ross, Organismal Biology and Anatomy, University of Chicago, 1027 East 57th Street, Chicago, IL 60637. Fax: 773-702-0037. E-mail: rossc@uchicago.edu

Received 12 January 2005; Accepted 13 January 2005
DOI 10.1002/ar.a.20170
Published online 3 March 2005 in Wiley InterScience (www.interscience.wiley.com).

TABLE 1. Physiological cross-sectional areas of the masticatory muscles of *Macaca* in cm^2

	Anterior temporalis	Deep masseter	Medial pterygoid	Superficial masseter
Macaca mulatta	1.62	1.3	2.12	3.36
Macaca fuscata	1.62	1.44	4.43	3.28
Macaca fascicularis	1.62	1.08	1.45	1.56
Genus average	1.62	1.273	2.666	2.733

pithecus, can provide useful insight into how those skulls functioned in life. The validity of these models cannot be assessed by gathering in vivo data. Rather, their validity is a function of the validity of the methods used to construct and load them. What can we say about how the australopithecine skull functioned if we have good data on skull geometry from fossils, but no direct data on either material properties of the bone, the size of the masticatory muscles, or the manner in which the muscles are recruited? This aim of our research has application to vertebrate taxa, extant and extinct, for which in vivo data cannot be gathered, as well as to intermediate forms not represented by fossils, but synthesized or estimated using algorithms modeling morphological evolution. What does one need to know to build and load a useful FEM?

In a companion article in this issue, Strait et al. (2005) address this question by looking at variation in strain orientations and magnitudes associated with variation in the material properties in our macaque skull model while holding the external forces constant. The present contribution investigates the effects of altering various parameters underlying our estimates of external (masticatory muscle) forces while holding geometry and material properties constant. We also suggest a new technique for summarizing overall differences in model behavior resulting from these altered conditions.

Muscle Force Estimates in Finite Element Analysis (FEA)

The relative magnitudes of the external forces estimated for the masticatory muscles are fundamental to the loading regime in the model. Although we do not know how accurate these force estimates are, it is possible to evaluate their relative influence using a sensitivity analysis of the assumptions made in their calculation. This article presents the results of a sensitivity analysis of the behavior of the model under different assumptions regarding the relative and absolute magnitudes of the external muscle forces applied to it.

The principal external forces applied to the skull during mastication and biting are the bite, masticatory muscle, and joint reaction forces (although muscle forces act on the nuchal plane and reaction forces act on the foramen magnum during mastication, these forces can be ignored in the present instance because they and their associated moments oppose each other and are resolved within the skull posterior to the occipital condyles). Our method for modeling these forces is to use in vivo electromyographic (EMG) data to estimate the proportions of muscle physiological cross-sectional area recruited, and to apply these forces to the attachment areas of the muscles on the skull. The model is held in static equilibrium by constraining nodes at the temporomandibular joint (TMJ) and first molar. In this manner, the skull is effectively pulled down onto the bite point and TMJ, thereby generating reaction forces in these areas that are functions of muscle force magnitudes, positions, and orientations.

Physiological cross-sectional area. The first aim of this study is to investigate the effect of variation in estimates of physiological cross-sectional area (PCSA) on the loading regime of the FEM. The estimates of external muscle forces are derived using estimates of PCSA of the jaw muscles of several species of macaque available in the literature (Anton, 1999, 2000). The PCSA values are estimates of the total amount of force that each muscle can generate; as discussed below, in vivo EMG data gathered by us provide an estimate of how much of that PCSA is recruited.

Estimating the PCSA of jaw muscles is a difficult and time-consuming task, data are only available for a handful of primates (Schumacher, 1961; Anton, 1999, 2000), and the relationship between the PCSA estimates and force production is poorly documented. Our FEM was constructed using CT data from an adult male *Macaca fascicularis* specimen and our EMG data were collected from an adult female *Macaca mulatta*, so we investigated the effect of using PCSAs from three different species of *Macaca* and a genus average (Table 1) (Anton, 1999, 2000).

Scaling PCSA. The second aim of this study is to investigate the effects on the FEM loading regime of different assumptions regarding the scaling of PCSA recruitment. Two approaches were taken. The first, the percentage scaling approach, scales the PCSAs of all of the chewing muscles to three different equal proportions: 100%, 50%, and 25%. This might be the approach taken when modeling force levels in fossil species when information on relative recruitment levels is not available. It might also be preferred if the relationship between EMG amplitudes of individual jaw muscles and bite force during mastication is weak or difficult to characterize (Ahlgren and Öwall, 1970; Proeschel and Morneburg, 2002). This has been attributed to the fact that during mastication there are changes in shortening velocity and length of the masticatory muscles and under these circumstances muscle force is not well correlated with EMG amplitudes (Ralston, 1961; Ahlgren and Öwall, 1970; Weijs, 1980). The percentage scaling approach investigates the effect on the FEM of assuming equal percentage recruitment of all masticatory muscles.

The second approach to investigating effects of PCSA recruitment, the EMG scaling approach, uses root mean square (r.m.s.) EMG data to scale the proportions of PCSA input into the model. Some researchers have argued that the lack of correlation between individual muscle EMGs and bite force does not reflect the lack of a relationship between overall muscle EMG and masticatory bite force,

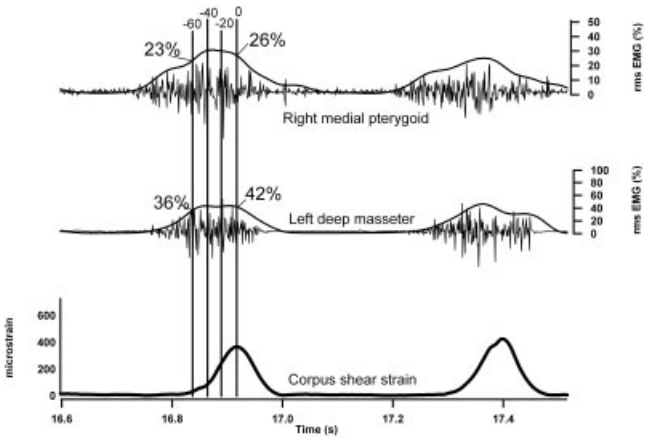

Fig. 1. Raw and r.m.s. EMG traces for the right medial pterygoid and left deep masseter muscles and left corpus bone strain data recorded from *Macaca mulatta* during two chews on apple on the left side. This figure illustrates how peak EMG activity in any given masticatory muscle is not necessarily synchronous with peak activity in other muscles, nor with peak strain in the mandibular corpus. 0, time when corpus strain peaks during the power stroke; −20, 20 msec prior to peak corpus strain; −40, 40 msec prior to peak corpus strain; −60, 60 msec prior to peak corpus strain; r.m.s. EMG values are expressed as percentage of maximum activity recorded during the experiment; % values indicated illustrate that the relative magnitude of r.m.s. EMG estimated for a muscle varies depending on time relative to peak corpus strain.

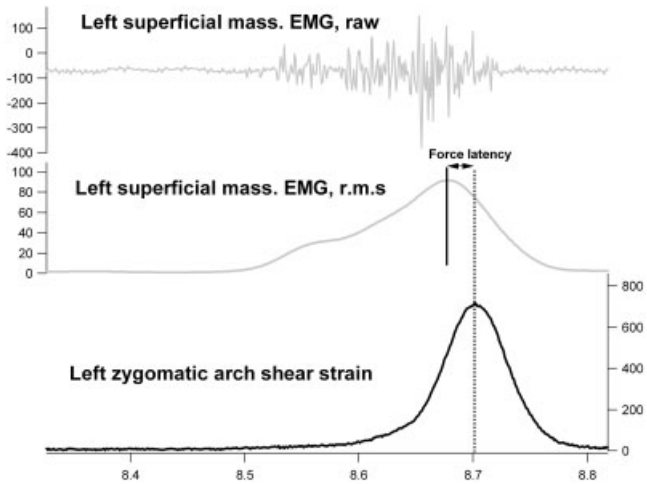

Fig. 2. Temporal relationship between raw and r.m.s. EMG from the superficial masseter muscle and bone strain in the zygomatic arch. Top trace illustrates raw EMG data recorded from the superficial masseter; middle trace illustrates the r.m.s. EMG signal; bottom trace is shear strain recorded from the zygomatic arch. EMG and strain data are recorded simultaneously from a macaque during mastication. The latency between peak EMG and peak shear strain in the arch is used to estimate the latency between EMG and force in the masticatory muscles (Hylander and Johnson, 1993).

but a failure to measure adequately either the bite force produced at all points in the tooth row or the EMG activity of the muscles of mastication (Ahlgren and Öwall, 1970; Hylander and Johnson, 1989). For example, Hylander and Johnson (1993) demonstrated a significant correlation between r.m.s. EMG amplitudes in the superficial masseter muscle and strain magnitudes in the zygomatic arch of macaques. Moreover, masticatory muscle EMG amplitudes are correlated with bite force during isometric biting (Pruim et al., 1978, 1980; Lindauer et al., 1993; Mao and Osborn, 1994) and rhythmic open-close movements against simulated food resistance (Ottenhoff et al., 1996) and are modulated to food texture (Blanksma and Vaneijden, 1995), even within the first power stroke of a chewing sequence (Ottenhof et al., 1993; Peyron et al., 2002). Thus, use of r.m.s. EMG data to estimate the proportion of PCSA being recruited may be a reasonable approximation of the force generated.

If r.m.s. EMG values are used to scale the PCSAs input into the model, at what time during the power stroke should the r.m.s. EMG values be measured? We are currently modeling the behavior of the macaque skull at the time during the power stroke when bite force is maximal, as estimated using bone strain magnitudes measured from the mandibular corpus (Weijs, 1980; Hylander,

Fig. 3. Plot of mean latency (± 1 SD) between muscle stimulation and contraction of motor units, muscle bundles, and whole masticatory muscles of various mammals. Plot also includes unpublished data and data from Hylander and Johnson (1989) on mean latency between EMG and bone strain measured with strain gauges, and data from other workers on mean latency between EMG and force measured at the teeth with a bite force transducer. Data sources: single motor unit stimulation data in rabbit masseter (Kwa et al., 1995); whole muscle stimulation of rabbit masseter (Guelinckx et al., 1986) and digastric (Muhl et al., 1978); muscle bundle stimulation of *Felis* masseter and temporalis (Tamari et al., 1973; Taylor et al., 1973); whole muscle stimulations of *Felis* muscles (MacKenna and Turker, 1978); whole muscle stimulations of *Didelphis* (Thexton and Hiiemae, 1975); whole muscle stimulations of *Sus* (Anapol and Herring, personal communication); single motor unit EMG and bite force in *Homo sapiens* masseter (Goldberg and Derfler, 1977); anterior temporalis EMG and bite force (Hannam et al., 1975); anterior temporalis and masseter EMG and bite force in *Homo sapiens* (Ahlgren and Öwall, 1970); *Macaca mulatta* muscle bundle stimulations in temporalis and superficial masseter (Faulkner et al., 1982); *Macaca mulatta* temporalis motor unit EMG and bite force (range only) (Clark et al., 1978); stimulation of all masticatory muscles and bite force measurement in *Macaca mulatta* (Dechow and Carlson, 1990); superficial masseter EMG (surface electrodes) and zygomatic arch bone strain in *Macaca fascicularis* (Hylander and Johnson, 1989); superficial masseter EMG (surface electrodes) and zygomatic arch bone strain in *Macaca mulatta* (Ross and Patel, unpublished data); superficial masseter EMG (indwelling electrodes) and postorbital septum bone strain in *Macaca mulatta* (Ross and Patel, unpublished data); anterior temporalis EMG (indwelling electrodes) and postorbital septum bone strain in *Macaca mulatta* (Ross and Patel, unpublished data); anterior temporalis EMG (indwelling electrodes) and temporal line bone strain in *Macaca mulatta* (Ross and Patel, unpublished data). Symbols represent mean values; lines represent ± 1 SD in all cases except data from Clark et al. (1978), where the lines represent the range. B, balancing; W, working; ant. temp., anterior temporalis; line, temporal line; septum, intraorbital surface of lateral orbital wall; sup. mass., superficial masseter; mast. mm., masticatory muscles; temp., temporalis; mass., masseter; dig., digastric; med. pt., medial pterygoid; post. temp., posterior temporalis; mid. temp., middle temporalis.

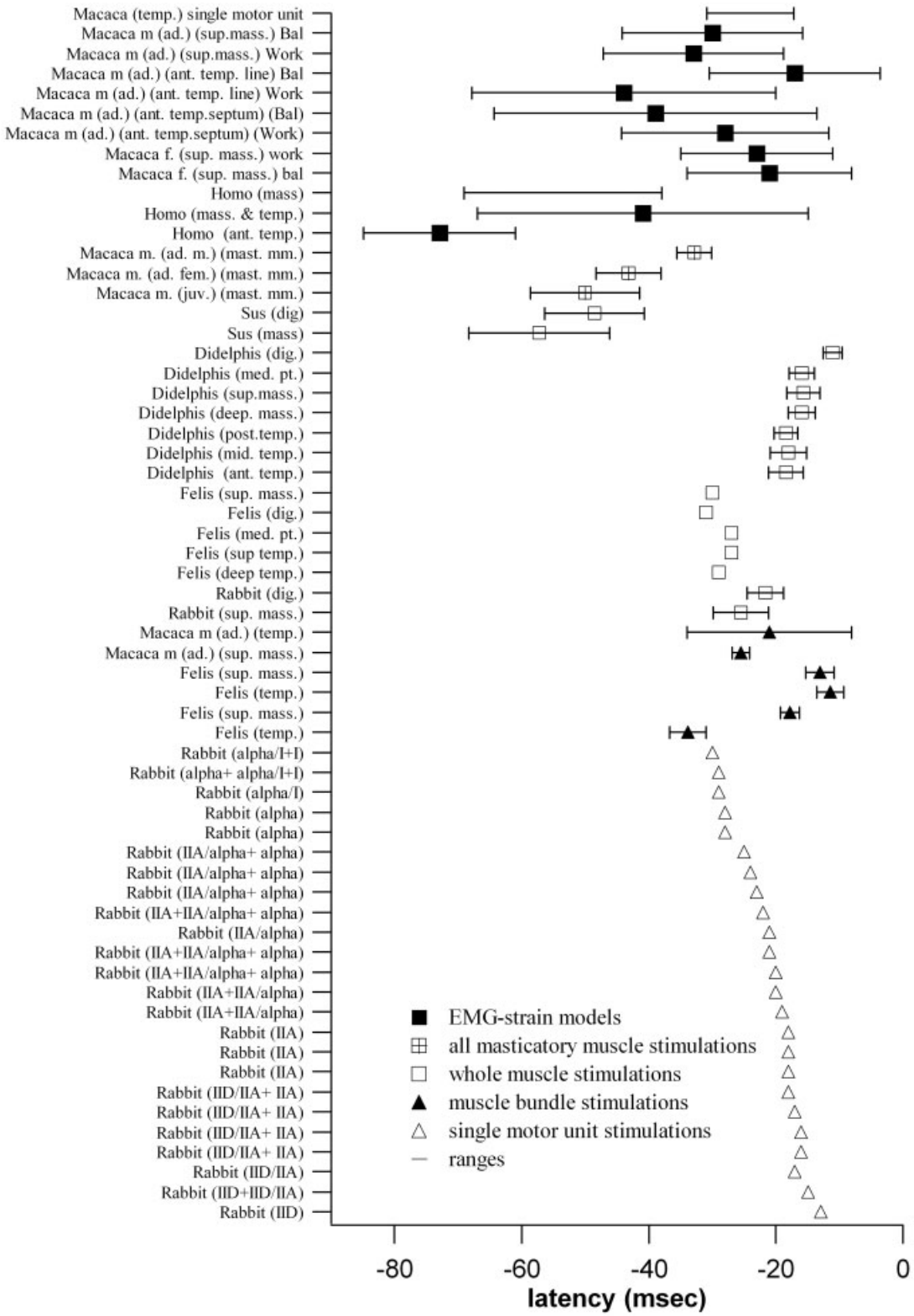
Macaca (temp.) single motor unit
Macaca m (ad.) (sup.mass.) Bal
Macaca m (ad.) (sup.mass.) Work
Macaca m (ad.) (ant. temp. line) Bal
Macaca m (ad.) (ant. temp. line) Work
Macaca m (ad.) (ant. temp.septum) (Bal)
Macaca m (ad.) (ant. temp.septum) (Work)
Macaca f. (sup. mass.) work
Macaca f. (sup. mass.) bal
Homo (mass)
Homo (mass. & temp.)
Homo (ant. temp.)
Macaca m. (ad. m.) (mast. mm.)
Macaca m. (ad. fem.) (mast. mm.)
Macaca m. (juv.) (mast. mm.)
Sus (dig)
Sus (mass)
Didelphis (dig.)
Didelphis (med. pt.)
Didelphis (sup.mass.)
Didelphis (deep. mass.)
Didelphis (post.temp.)
Didelphis (mid. temp.)
Didelphis (ant. temp.)
Felis (sup. mass.)
Felis (dig.)
Felis (med. pt.)
Felis (sup temp.)
Felis (deep temp.)
Rabbit (dig.)
Rabbit (sup. mass.)
Macaca m (ad.) (temp.)
Macaca m (ad.) (sup. mass.)
Felis (sup. mass.)
Felis (temp.)
Felis (sup. mass.)
Felis (temp.)
Rabbit (alpha/I+I)
Rabbit (alpha+ alpha/I+I)
Rabbit (alpha/I)
Rabbit (alpha)
Rabbit (alpha)
Rabbit (IIA/alpha+ alpha)
Rabbit (IIA/alpha+ alpha)
Rabbit (IIA/alpha+ alpha)
Rabbit (IIA+IIA/alpha+ alpha)
Rabbit (IIA/alpha)
Rabbit (IIA+IIA/alpha+ alpha)
Rabbit (IIA+IIA/alpha+ alpha)
Rabbit (IIA+IIA/alpha)
Rabbit (IIA+IIA/alpha)
Rabbit (IIA)
Rabbit (IIA)
Rabbit (IIA)
Rabbit (IID/IIA+ IIA)
Rabbit (IID/IIA+ IIA)
Rabbit (IID/IIA+ IIA)
Rabbit (IID/IIA+ IIA)
Rabbit (IID/IIA)
Rabbit (IID+IID/IIA)
Rabbit (IID)
EMG-strain models
all masticatory muscle stimulations
whole muscle stimulations
muscle bundle stimulations
single motor unit stimulations
ranges
-80
-60
-40
-20
0
latency (msec)

Figure 3.

1986). One possible approach is to use the highest r.m.s. EMG values recorded from each muscle during a power stroke. However, in primates (including humans), the muscles of mastication display peak activity at different times during the chewing cycle (Hylander et al., 1987, 2000), with some peaking after and some well before the time of peak bite force (Fig. 1). Not all of these muscles contribute equally to generation of peak bite force because they do not exhibit peak EMG activity at the same time.

Nor is it reasonable to use the r.m.s. EMG values recorded simultaneous to peak strain in the mandibular corpus because there is a delay between muscle EMG activity and force production (Fig. 2). This delay is due to the latent period between excitation of a muscle fiber and cross-bridge contraction and to elastic components of the connective tissue and tendons in series with the muscle fibers (Weijs and Van Ruijven, 1990). This EMG-force latency varies with muscle fiber type, muscle architecture, and muscle length (Inman et al., 1952; Faulkner et al., 1982; Woittiez et al., 1984; Loeb and Gans, 1986; Hylander and Johnson, 1989, 1993), suggesting that different masticatory muscles might exhibit different latencies, or that the same muscle might exhibit different latencies at different times during the masticatory cycle.

The EMG-force latency period in masticatory muscles has been estimated in a number of species using the time to peak tension (TPT) measured during stimulation of individual motor units (Kwa et al., 1995), fiber bundles (Thexton and Hiiemae, 1975; Faulkner et al., 1982), individual muscles (Thexton and Hiiemae, 1975; Muhl et al., 1978; Guelinckx et al., 1986), or the masticatory muscles as a whole (Dechow and Carlson, 1990). These methods measure different phenomena and yield different results, even within a single species (Fig. 3). For example, in female *Macaca mulatta*, mean times to peak twitch tension of 22 and 26 msec were measured in vitro by stimulating muscle fiber bundles extracted from temporalis and masseter (Faulkner et al., 1982). In contrast, a time to peak twitch tension of 43.2 msec was measured in vivo during stimulation of masseter, temporalis, and medial pterygoid muscles (Dechow and Carlson, 1990). This variation in latency between EMG stimulation and force production in masticatory muscles reflects differences in muscle architecture, fiber type, patterns of recruitment, and experimental technique. The relevance of these muscle stimulation studies for estimating the EMG-force latency during mastication is not clear. Proeschel and Morneberg (2002) have demonstrated that EMG-force relationships established during isometric biting are only indirectly related to forces during mastication. Whether this effect also applies to EMG-force latencies is not clear.

Problems associated with muscle stimulation data can be avoided by estimating the EMG-force latency in masticatory muscles during mastication using EMG data and some measure of force production, either at the bite point or in the bones adjacent to the muscle attachments. Clark et al. (1978) measured the latency between EMG activity in 24 individual motor units in the superficial middle temporales of two alert subadult male *Macaca mulatta* and isometric bite force measured with a transducer on the incisors, obtaining values ranging from 17 to 31 msec. Hylander and Johnson (1989) measured the latency between zygomatic arch bone deformation measured with strain gauges and superficial masseter EMG measured with surface electrodes in six macaques during mastication of apple with skin. They report a range of latencies, with grand means ranging from 26 to 37 msec on the working side and from 29 to 52 msec on the balancing side. Our own data on superficial masseter EMG-zygomatic arch strain latencies in macaques range from 10 to 62 msec and our data on anterior temporalis EMG-temporal line bone strain latencies range from 10 to 69 msec (Ross and Patel, 2003).

Thus, there is variability in EMG-force latency related to differences in EMG sampling (single versus multiple motor units), muscle identity (masseter versus temporalis), feeding activities being performed (isometric biting versus mastication), and methods of force measurement (bite force transducer versus strain gauges). What is not clear is whether varying assumptions regarding this latency have a significant effect on the behavior of the FEM. To address this issue, we assessed the sensitivity of the model to use of six different EMG-force latency periods, bracketing the range of values reported in the literature, and measured by us: 10, 20, 30, 40, 50, and 60 msec prior to the time of peak corpus shear strain (Fig. 1).

In sum, this study assesses the sensitivity of the FEM to assumptions regarding species-specific variation in PCSA and the degree to which that PCSA is recruited during mastication.

MATERIALS AND METHODS

PCSA

Values for PCSA of the masticatory muscles were taken from Anton's (1999, 2000) work on genus *Macaca*. PCSA values for superficial masseter, deep masseter, medial pterygoid, and anterior temporalis muscles for *M. mulatta*, *M. fascicularis*, and *M. nemestrina* were taken from Anton (1999, 2000), and a genus average was also calculated (Table 1). The only available anterior temporalis data are for *Macaca fuscata*. These data were used for all species. The data correspond to Anton's part 1 (1993). The medial pterygoid data are from Anton (2000: p. 136, Table II, MPPCS); the masseter data are from Anton (1999: p. 446, Table II), with deep masseter corresponding to part C and superficial masseter to the sum of parts B, Y, and F.

EMG Scaling of PCSA

One adult female *Macaca mulatta* with a fully erupted dentition served as a subject. With the animal under isofluorane anesthesia, indwelling fine-wire electrodes were placed bilaterally in the anterior temporalis, superficial masseter, deep masseter, and medial pterygoid muscles. Electrodes in the anterior temporalis were placed 1 cm inferior to the anterior temporal line by inserting the needle in a coronal plane at an angle of approximately 45° to the sagittal plane until it contacted bone. Electrodes were placed in the central portion of the superficial masseter, approximately 1 cm from the inferior border of the mandible, in the medial pterygoid muscle in the same coronal plane as the superficial masseter, also approximately 1 cm from the inferior border of the mandible, and in the posterior part of the deep masseter immediately anterior to the TMJ. After placement of EMG electrodes, a delta rosette strain gauge was glued to the left mandibular corpus below M1 following the procedures in Ross (2001). (Three other gauges were placed during this experiment, but the data are not presented here.)

After placement of EMG electrodes and strain gauges, the animal was restrained in a chair with the head and

neck able to move freely, woken from anesthesia, and presented with various foods. While the animal chewed, EMG and strain data were acquired at 2.7 KHz using the telemetry system described by Stern et al. (1976) and the data acquisition system described in Ross (2001). At the end of each recording session, the animals were again anesthetized with isofluorane, the EMG electrodes and strain gauges were removed, and the animal was returned to its cage.

The EMG and strain data were imported into IGOR Pro 4.04 (Oswego, OR) for analysis using custom-written macros. EMG signals were Butterworth-filtered (band-pass 300–1,000 Hz) and quantified using an r.m.s. algorithm with a 42-msec time constant in 2-msec increments following Hylander and Johnson (1993). The r.m.s. EMG data were scaled so that the largest EMG value recorded during the experiment was assigned a value of 1.0 and the rest of the values were scaled linearly.

The raw strain data were used to calculate maximum (ε_1) and minimum (ε_2) principal strains following Ross (2001). ε_1-ε_2, the absolute maximum shear strain, or γ_{max} (Hibbeler, 2000) was calculated as a measure of overall strain magnitude (Hylander, 1979).

Right- and left-side power strokes were identified from videos of the experiments and muscle firing patterns. Because our model is loaded with the bite point on the left, only data from left chews were used and the left-side muscles were designated as the working-side and the right-side muscles were designated as the balancing side.

For eight sequences of apple mastication, the timing of peak γ_{max} in each power stroke was calculated. Then, for each power stroke, the scaled r.m.s. EMG value calculated for each of the eight muscles 10 msec prior to the time of peak strain was extracted. The mean of all power strokes was calculated, and this mean was used to scale the PCSA values. This procedure was repeated to calculate the mean r.m.s. EMG value for each muscle at 20, 30, 40, 50, and 60 msec prior to peak corpus strain.

Loading Model

The procedures for building and loading the FEM are described elsewhere (Strait et al., 2002, 2005, this issue). Briefly, a three-dimensional (3D) FEM of a male crab-eating macaque (*Macaca fascicularis*) skull was constructed from serial computed tomography (CT) scans. Using commercially available CAD software the CT scans were digitized, linked, and smoothed to produce a realistic model preserving both internal and external geometry. This 3D model was then imported into the finite-element software FEMPRO (Algor) and a solid mesh was created of brick elements at a size of 40%. The final mesh consisted of 145,680 elements and 55,956 nodes. Because the skull is not perfectly symmetrical, the mesh resulted in a different number of nodes, elements, and nodal values on each side (i.e., working and balancing sides).

To load the model, the forces estimated for the anterior temporalis, deep masseter, medial pterygoid, and superficial masseter muscles were divided evenly across the nodes underlying the muscle attachment area. An exception to this method was adopted when modeling the anterior temporalis. To replicate the fact that a large number of muscle fibers are attached to the temporalis fascia, and this presumably means that are higher along the temporal lines than across the rest of the muscle's origin, forces were applied to every node along the temporal lines and the zygomatico-mandibularis crest (Ross, 1995), but forces were only applied to a selection of evenly spaced nodes across the rest of the surface. This distribution of vectors has the effect of concentrating relatively more force along the lines and crests.

A total of 36 different loading regimes, or experiments, was run (Table 3): four different PCSA sets (three macaque species and a genus average); and nine different PCSA scaling parameters, consisting of six latency sets (10, 20, 30, 40, 50, and 60 msec) and three percentage sets (100%, 50%, and 25%). All 36 possible combinations were run.

Data Extracted From Model

Rather than extract data for every node in the model, data were extracted from 8,379 surface nodes in the face. This is the area of the skull that is best studied in terms of in vivo bone strain data.

FEA software allows various data to be extracted for each node, such as the orientations and magnitudes of principal stresses and strains, as well as derivatives of those basic variables, such as Von Mises stresses and strain energy density. Comparisons of global sums or averages of these variables are difficult to interpret, whereas local sampling of subsets of the nodes may fail to give an accurate picture of overall model behavior. In seeking to compare the behavior of the whole face under different loading regimes, principal coordinates methods were invoked. Because our FEA software easily outputs not only the x-, y-, z-coordinates of the nodes in the unloaded model, but also those of the loaded or deformed model, it was a simple exercise to extract the nodal coordinates of the model both in its unloaded condition and after deformations produced by the 36 different load sets. This enabled the quantitative and graphic representation of the relationships between experimental outcomes within the highly multidimensional space of vertex coordinates.

In many studies, principal components analysis (PCA) is used to provide a low-dimensional summary of experimental outcomes that best (in a least-squares sense) approximates the scatter of those outcomes in the full space of observed variables. This was impractical in the present case as it would require the decomposition of a $25{,}137^2$ sum-of-squares-and-cross-products (SSCP) matrix. Instead, we used the dual of this procedure, principal coordinates (PCOORD) analysis (Gower, 1966), to achieve the same ordination with considerably less computation. The PCOORD analysis produces the same ordination plots (up to arbitrary axis reflections) as a principal components analysis. PCOORD analyses only lack the variable loadings obtained in PCA that relate the sample variation to the original variables.

PCA can be achieved by the singular-value decomposition of the SSCP matrix of the (usually) mean-centered data matrix: $X^tX = ELE^t$, where X is the $n \times m$ matrix of m mean-centered vertex coordinates for n FEM experiments, and t represents the matrix transpose. E is an orthonormal matrix of the principal component variable loadings, and L is a diagonal matrix of their associated eigenvalues. The eigenvalues can be examined to assess how much of the variation between experiments can be expressed in a lower-dimensional subspace of the original variables. The data can be projected onto axes associated with the largest eigenvalues (the associated columns of E) to provide low-dimensional plots that best represent the

scatter of the data. In the present case, n = 37 (the unloaded vertices and results of 36 FEM experiments) and m = 3 × 8,379 = 25,137, making X^tX a 25,137 × 25,137 matrix. Most of these results, however, can be obtained by PCOORD, which decomposes not the coordinate SSCP matrix, but the interexperimental SSCP matrix: $XX^t = UDU^t$, where X is as before, U is an orthonormal matrix of principal coordinates, and D is a diagonal matrix of eigenvalues proportional to the variance of the data on each principal coordinate. Note that here we are working with an n × n = 37 × 37 matrix. In both PCA and PCOORD, the maximum number of components associated with nonzero eigenvalues (variance) will be the minimum of m and n − 1. In our case, this means a maximum of 36 possible principal components or principal coordinate axes.

The columns U multiplied by $D^{1/2}$ are, up to reflections, the same coordinates and produce the same plots as the projection of the original data onto the principal components axes. All that is lost are the loadings of individual variables contained within the principal components themselves.

In order to relate the PCOORD results to the external forces acting on the model, the principal coordinates were regressed against the muscle forces modeled in the 36 different experiments. Partial regression coefficients were used to quantify the relative effects of the different muscles on variation in the principal coordinates of the 36 experiments.

The results of the sensitivity analyses were also compared with in vivo strain data recorded from eight sites on the facial bones of *Macaca mulatta* and *Macaca fascicularis* (Hylander et al., 1991; Hylander and Johnson, 1997; Ross, 2001). The orientation of the maximum principal strain (ε_1), the magnitude of the maximum shear strain (γ_{max}), and the ratio of maximum (ε_1) to minimum (ε_2) principal strains recorded in vivo were compared with the data obtained from similar sites on the model. The in vivo strain data are presented as the grand mean of all reported data ± 2 SD (see Strait et al., 2005, this issue).

RESULTS

The PCOORD analysis revealed that most of the experimental variation can be expressed in two principal coordinates, with the first principal coordinate axis accounting for approximately 94% of the total variation, and the first two accounting for nearly 100%. This suggests that little information about the variation in experimental results is lost by examining plots of these results in the space of the first two PCOORD axes (Fig. 4). In Figure 4, the coordinates of the unstressed model are on the far left, with the coordinates of the 36 loaded models leading off to the right along two distinct vectors approximately 0.25 radians (14.7°) apart.

The first vector, roughly parallel to the first principal coordinate, is constituted by the 12 loading regimes representing simple percentage scaling of PCSA (experiments 25–36; Table 2). This vector runs in a nearly straight line from the unloaded model to the experiment resulting in the greatest deformation, experiment 26. The experiments in which higher percentages of muscle PCSA were recruited are located further to the right along this vector, irrespective of the species from which PCSA was estimated.

The second vector represents the results of the remaining experiments, in which PCSA was scaled according to

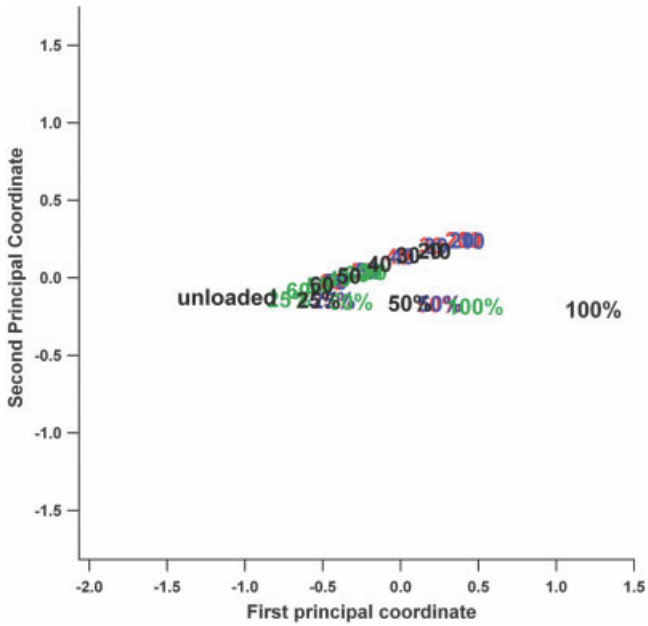

Fig. 4. Bivariate plot of first and second principal coordinates of the unloaded and the 36 loaded models produced by the 36 different experiments listed in Table 2. Unloaded, the coordinates of the unloaded model; 25%, 50%, 100%, coordinates of the model loaded by recruiting 25%, 50%, and 100% of the PCSA of the masticatory muscles (i.e., percent scaling loading regimes); 10, 20, 30, 40, 50, 60, coordinates of the model loaded by recruiting the PCSA proportionate to the r.m.s. EMG recorded 10, 20, 30, 40, 50, 60 msec prior to peak strain in the mandibular corpus (i.e., EMG scaling loading regime).

r.m.s. EMG values recorded at 10, 20, 30, 40, 50, and 60 msec prior to peak mandibular corpus strain. Again, these results lie along a more or less straight line from the unloaded, undeformed model to the experimental result with the most extreme deformation, experiment 7 (Fig. 4). The experiments with the shortest latencies lie furthest from the unloaded model along this vector, and further along both PCOORD1 and PCOORD2, while the longest latencies are found closer to the unloaded model.

Multiple regression of the muscle forces applied to the model across the 36 experiments against the first two principal coordinates produced the partial regression coefficients listed in Table 3 (we use the term "multiple regression" here only to relate the arrangement of experimental outcomes shown in Figure 4 to the relative patterns of muscle force inputs; the details of the regression results for each PCOORD apply only to the current set of experiments, and other mixtures of inputs could alter the orientations of the PCOORD axes). In both cases, the overall r^2 was 1.00, indicating that 100% of the variance in PCOORD1 and PCOORD2 is explained by differences in muscle recruitment level.

The coefficients reveal positive relationships between the degree of muscle recruitment and PCOORD1 in all but the working-side medial pterygoid (Table 3). Thus, in most instances, increased recruitment of the muscles is associated with higher loading in PCOORD1. The highest coefficients are those for the balancing-side masseters, followed by the working-side masseters, then the balancing- and working-side temporalis muscles. The coefficients for

TABLE 2. Combinations of PCSA and latency periods constituting the 36 different load sets used in this study

Experiment #	PCSA	Latency/% scaling
1	*M. mulatta*	10 msec
2	*M. mulatta*	20 msec
3	*M. mulatta*	30 msec
4	*M. mulatta*	40 msec
5	*M. mulatta*	50 msec
6	*M. mulatta*	60 msec
7	*M. fuscata*	10 msec
8	*M. fuscata*	20 msec
9	*M. fuscata*	30 msec
10	*M. fuscata*	40 msec
11	*M. fuscata*	50 msec
12	*M. fuscata*	60 msec
13	*M. fascicularis*	10 msec
14	*M. fascicularis*	20 msec
15	*M. fascicularis*	30 msec
16	*M. fascicularis*	40 msec
17	*M. fascicularis*	50 msec
18	*M. fascicularis*	60 msec
19	*Macaca* average	10 msec
20	*Macaca* average	20 msec
21	*Macaca* average	30 msec
22	*Macaca* average	40 msec
23	*Macaca* average	50 msec
24	*Macaca* average	60 msec
25	*M. mulatta*	100%
26	*M. fuscata*	100%
27	*M. fascicularis*	100%
28	*Macaca* average	100%
29	*M. mulatta*	50%
30	*M. fuscata*	50%
31	*M. fascicularis*	50%
32	*Macaca* average	50%
33	*M. mulatta*	25%
34	*M. fuscata*	25%
35	*M. fascicularis*	25%
36	*Macaca* average	25%

TABLE 3. Partial regression coefficients from multiple regression of muscle force estimates against the first two principal components

	PCOORD1	PCOORD2
Intercept	−1.1200000	−0.1250000
Working anterior temporalis	0.0010500	0.0005250
Working deep masseter	0.0064500	0.0079000
Working medial pterygoid	−0.0000040	−0.0000015
Working superficial masseter	0.0068000	0.0083000
Balancing anterior temporalis	0.0029400	−0.0021000
Balancing deep masseter	0.0093800	−0.0063100
Balancing medial pterygoid	0.0000007	−0.0000061
Balancing superficial masseter	0.0122000	−0.0090800

both balancing- and working-side medial pterygoids are very low, indicating that their degree of recruitment has little effect on the PCOORD1 score for each experiment.

Partial regression coefficients for regression on PCOORD2 reveal a different pattern (Table 3). In this case, all of the balancing-side muscles show negative coefficients, as does the working-side medial pterygoid; the remainder of the working side muscles show positive coefficients. The coefficients for the pterygoid muscles are very low; those for the remainder of the muscles are of similar magnitude but opposite sign on working and balancing sides.

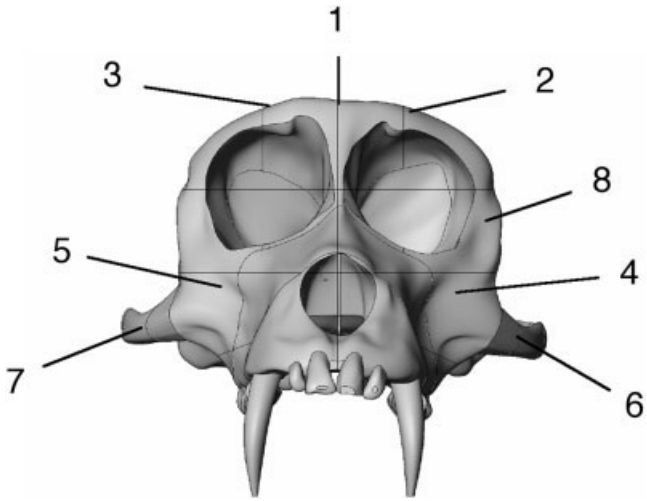

Fig. 5. Diagram illustrating locations of eight points from which bone strain data were sampled in vivo and from the finite-element model. 1, dorsal interorbital; 2, working dorsal orbital; 3, balancing dorsal orbital; 4, working infraorbital; 5, balancing infraorbital; 6, working anterior zygomatic arch; 7, balancing anterior zygomatic arch; 8, working-side postorbital bar.

Figure 5 illustrates the eight sites from which in vivo strain data are available for comparison with the data from the models. The maximum shear strain (γ_{max}) values recorded at the eight sites are plotted in Figure 6. The top plot in Figure 6 compares the in vivo data (grand mean and spread) with the results from the 12 experiments in which the PCSA values were scaled to equal percentages of total PCSA. The bottom plot in Figure 6 compares the in vivo data (grand mean and spread) with the results from the 24 experiments in which the PCSA values were scaled using r.m.s. EMG values recorded in vivo. The data from the models using r.m.s. EMG values more closely resemble the in vivo data in relative magnitudes of γ_{max} at the eight sites. The experiments that most closely resemble the in vivo results are experiments 7, 1, 8, and 2, respectively.

Figure 7 compares the ratios of maximum to minimum principal strains recorded in vivo with those obtained from the model. The ratios recorded from the model under the various loading regimes roughly correspond to those recorded in vivo, although there is no distinct difference between the results of the percentage scaling loading regimes and those involving the EMG scaling loading regimes.

The ranges of ε_1 orientations recorded from the eight sites in vivo are illustrated in Figure 8, with the ε_1 orientations obtained from the model under all 36 loading regimes superimposed in red. The orientation of ε_1 at the seven of the eight sites corresponds well with the ranges of ε_1 orientation recorded in vivo, falling within the in vivo range in all but two cases. Moreover, there is relatively little variation in ε_1 orientation across the 36 experiments, with the range always being much less than those reported from in vivo data.

DISCUSSION

This study investigated the sensitivity of our FEM of the macaque skull to changing assumptions regarding the

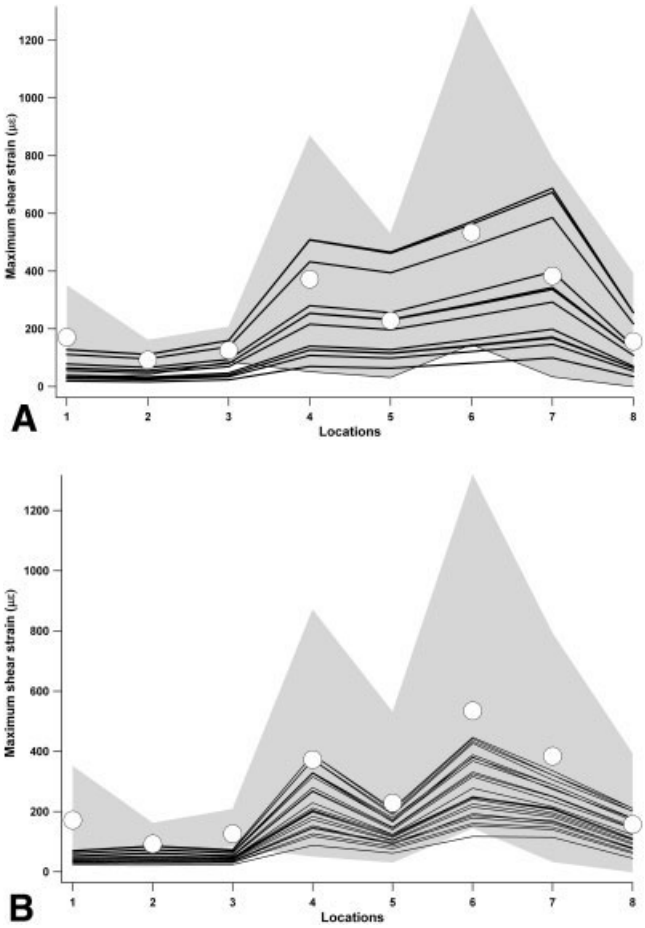

Fig. 6. Bivariate plot of maximum shear strain (γ_{max}) recorded in vivo and extracted from the FEM. The mean γ_{max} recorded at each site is indicated by circles; ± 2 SD is shaded. The results of the 36 loading experiments are shown in thin black lines. **A:** Results of the 12 percentage scaling experiments. **B:** Results from the 24 latency experiments.

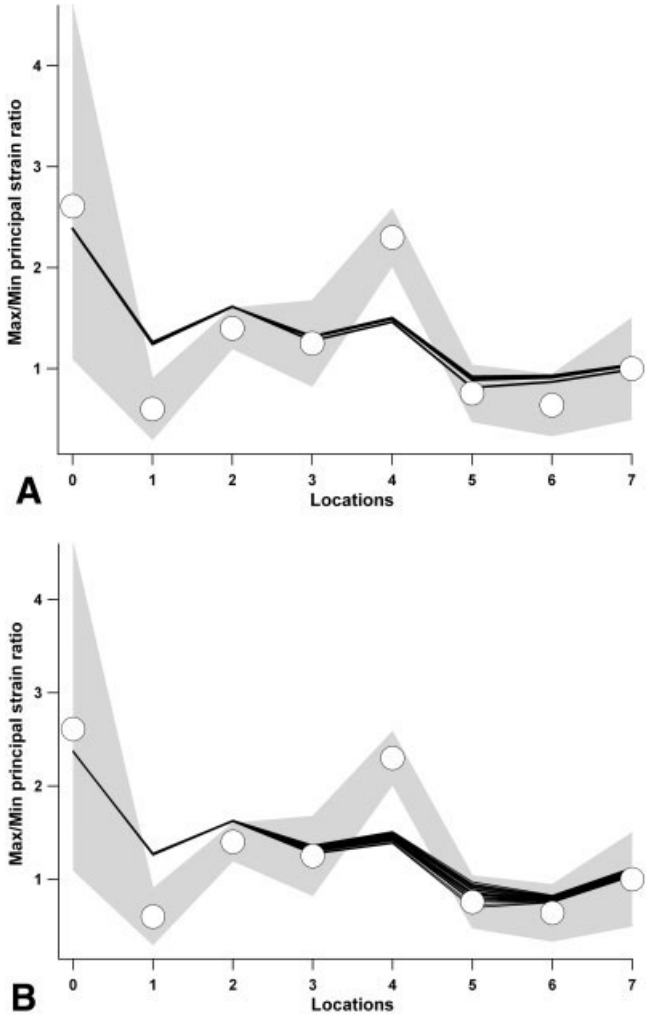

Fig. 7. Bivariate plot of $\varepsilon_1/\varepsilon_2$ ratios recorded in vivo and extracted from the FEM. The mean $\varepsilon_1/\varepsilon_2$ ratio recorded at each site is indicated by circles; ± 2 SD is shaded. The results of the 36 loading experiments are shown in thin black lines. **A:** Results of the 12 percentage scaling experiments. **B:** Results from the 24 latency experiments.

muscle forces loading the model. Specifically, we investigated the relative importance of the PCSAs assumed for the masticatory muscles and the proportions of the PCSAs being recruited.

PCOORD analysis revealed that almost all variations in model behavior were captured in the first two principal coordinates and, within the space defined by these two coordinates, the responses of the model fell along two vectors (Fig. 4).

The vast majority of the variation (94%) along both vectors lay along the first PCOORD, and several factors suggest that PCOORD1 describes variation in the amount of deformation of the model, rather than in the nature of the deformation. First, multiple regression analyses revealed that for all but one muscle, there was a significant positive relationship between the muscle force magnitudes and the value of PCOORD1. In addition, different relative positions of experiments along PCOORD1 roughly correspond to the relative magnitudes of overall muscle force, as estimated by PCSA, used in each experiment (cf. Tables 1 and 3): experiments in which the PCSAs of *Macaca mulatta* and *Macaca fuscata* were used to load the model lie further to the right, followed by the *Macaca* average, then *Macaca fascicularis*.

The ordering of the experimental results within the two vectors also suggests that greater deformations are associated with higher values of PCOORD1. Within the horizontal vector, controlling for the species PCSA being used, experiments in which a greater percentage of PCSA were recruited have higher values for PCOORD1. This is also the case within the oblique vector, as revealed by examination of Figure 1. The experiments with the highest values on PCOORD1 are those in which the shortest EMG-force latency was assumed (10 msec), whereas the experiments with the lowest values on PCOORD1 are those in which a long latency of 60 msec was assumed. As Figure 1 illustrates, when a long EMG-force latency of 60 msec is assumed, relatively small r.m.s. EMG amplitudes are measured because muscles are still in the early stages of recruitment 60 msec prior to peak corpus strain. The majority of EMG values increase up to about 10 msec prior

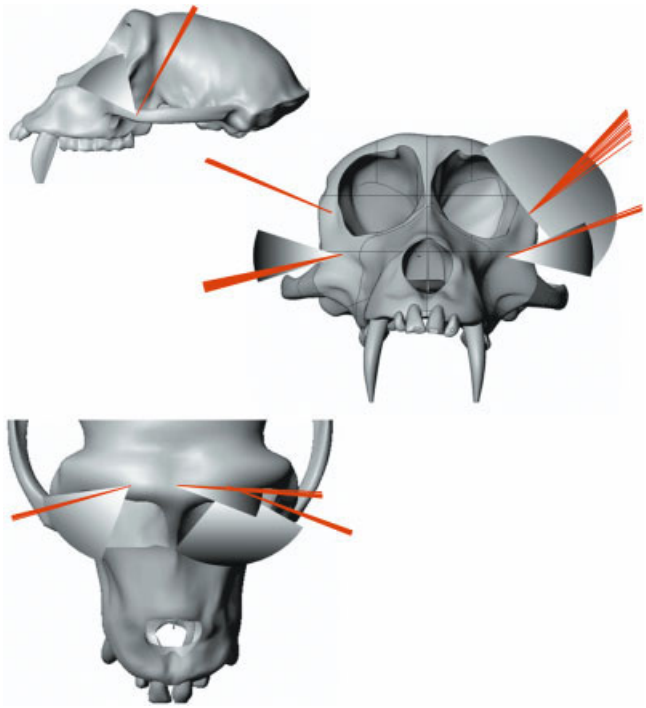

Fig. 8. Orientations of ε_1 recorded from the 36 loading experiments on the FEM compared with the range of values reported in vivo. The data from the 36 loading experiments are shown as red vectors. The length of the vectors is arbitrary.

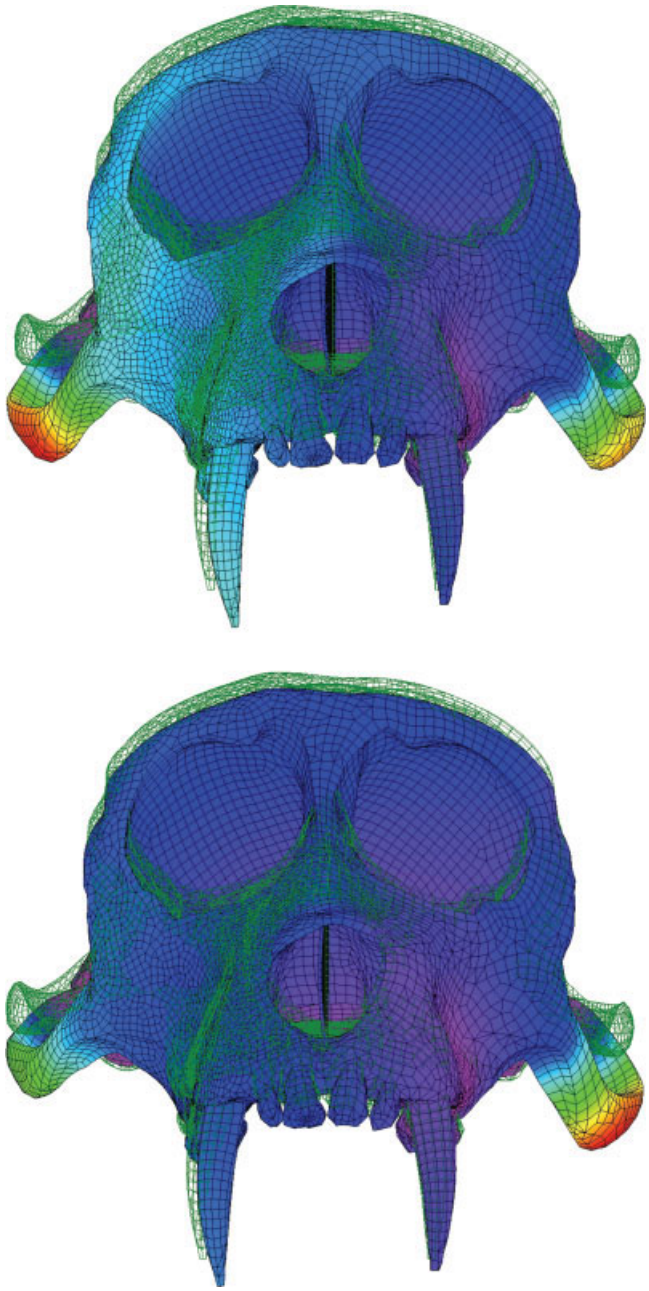

Fig. 9. Top: Pattern of deformation produced in experiment 26 by recruitment of 100% of the PCSA of *Macaca fuscata*. Bottom: Pattern of deformation produced in experiment 7, i.e., recruitment of the PCSA of *Macaca fuscata* according to r.m.s. EMG recorded only 10 msec prior to peak corpus strain. In both cases, the degree of deformation has been magnified 10 times. The unloaded mesh is shown in green.

to peak corpus strain, then decrease. Hence, longer assumed EMG-force latencies are associated with lower recruitment of PCSA and smaller overall forces acting on the model.

If PCOORD1 largely reflects the amount of force being applied to the model, what then is the significance of PCOORD2? Examination of the loading regimes associated with the extremes of the two vectors (Fig. 9) suggests that PCOORD2 primarily reflects variation in the nature of the loading regime. The top image in Figure 9 illustrates the pattern of deformation produced in experiment 26 by recruitment of 100% of the PCSA of *Macaca fuscata*. The bottom image in Figure 9 illustrates the pattern of deformation produced in experiment 7, i.e., recruitment of the PCSA of *Macaca fuscata* according to r.m.s. EMG recorded only 10 msec prior to peak corpus strain. In both cases, the degree of deformation has been magnified to make the pattern of deformation visible. The most notable difference between the two deformation regimes is the higher degree of asymmetry produced in experiment 7. Both models are asymmetrically loaded because the bite point is always on the left M1, but the muscle forces producing the deformation in the upper figure are symmetrical, whereas those producing the deformation in the bottom figure were much higher on the working than the balancing side. Thus, PCOORD2 can be hypothesized to expresses variation in cranial deformation associated with asymmetry in recruitment of masticatory muscles.

Returning to the original questions addressed in this study, it is noteworthy that differences in assumptions regarding the PCSAs of the muscles did not explain the differences between the two vectors in Figure 4: loading experiments using the four different PCSA combinations lie along both vectors. Rather, the primary determinant of the difference between the two vectors in PCOORD space is whether the model is loaded by scaling the PCSAs of all the muscles equally (i.e., percentage scaling), producing more symmetrical deformation, or whether r.m.s. EMG data are used to estimate the proportion of PCSA actually

recruited (i.e., EMG scaling), producing relatively asymmetrical deformation. It can therefore be argued that the nature of the deformation pattern produced in the model is more strongly affected by assumptions regarding relative recruitment levels of masticatory muscle PCSA than by precisely what those PCSA values are.

This suggests that if the aim of FEA is to precisely and accurately model the behavior of the skull at a particular instant during feeding, it is important to include estimates of the relative recruitment levels of the masticatory muscles. It is obviously not possible to obtain these data for extinct taxa, but there are several reasons to be optimistic about our ability to model fossil skull behavior precisely.

First, the high degree of working-balancing asymmetry characterizing the EMG values used here is characteristic of anthropoids only during mastication of soft food items, such as apple. Tougher food items elicit from anthropoids not only higher EMG amplitudes overall, but also working-balancing EMG ratios that more closely approach 1.0 (Hylander et al., 1998, 2004). Thus, the percentage loading sets applied in this study might better reflect the loading conditions acting on the anthropoid skull during mastication or biting of tough foods.

Second, this study did not seek to compare the behavior of the skull model under loads imparted by EMG recruitment patterns of animals other than macaques. It may be the case that patterns of loading produced by, for example, *Eulemur* EMG recruitment patterns during apple mastication more closely resemble those produced by *Macaca* EMG recruitment patterns during apple mastication than do the percentage loading sets applied here. We plan to explore the relative importance of interspecific differences in EMG recruitment patterns for patterns of skull loading in the future.

Another reason to be optimistic about our ability to model skull behavior in fossil taxa accurately and precisely derives from comparison of the strain orientation data derived from the model with that recorded in vivo (Fig. 8). It is clear from Figure 8 that the strain orientations recorded at the eight sites on the FEM not only generally fall within the range observed in vivo, but they also do not vary very greatly, suggesting that the nature of the loading regime in the model is relatively invariant across all 36 different loading conditions. This conclusion is also supported by the fact that PCOORD2 in Figure 4 (the principal coordinate associated with differences in the nature of deformation) only accounts for approximately 6% of the variance observed in the model. Most of the variation produced in these sensitivity analyses is in the magnitude of deformation, rather than its nature.

Why are strain orientations in the model much less variable than those reported from in vivo studies? The reasons for this lie in the much greater precision of the modeling results compared with the in vivo studies. The in vivo data derive from experiments performed on different animals, producing interexperiment variation in bone material properties, chewing behavior, and gauge placement. Moreover, many of the gauge locations and orientations are approximate due to problems with orientation and/or exposure of radiographs used to document gauge position. These problems are being corrected in current in vivo studies. However, it is clear from the problems arising during this study that in vitro studies of strain in artificially loaded specimens are an important and powerful tool for validating FEMs.

The problems notwithstanding, the relative invariance in the model's global loading regime across the 36 different experiments suggests that the nature of the loading regime in the model as a whole may be principally determined by the geometry of both the model and the external forces acting on it. The relative magnitudes of those forces are apparently of only secondary importance in determining global aspects of craniofacial loading. Given the general similarity between the behavior of our model and the apparent behavior of the skull in vivo, it is tempting to hypothesize that this may also be true of primate skulls in general. More detailed work on more circumscribed areas of the skull is needed to determine the extent to which this conclusion applies at smaller scales.

ACKNOWLEDGMENTS

Supported by grants from the National Science Foundation Physical Anthropology BCS 9706676 (to C.F.R. and X. Chen) and BCS 0240865 (to D.S.S., P.C.D., B.G.R., C.F.R., and M.A.S.). The workshop at which this article was originally presented was made possible by generous funding from the International Society of Vertebrate Morphologists, *The Anatomical Record*, and the Department of Organismal Biology and Anatomy at the University of Chicago. The critical comments of Fred Anapol, Betsy Dumont, and Paul O'Higgins improved the manuscript.

LITERATURE CITED

Ahlgren J, Öwall B. 1970. Muscular activity and chewing force: a polygraphic study of human mandibular movements. Arch Oral Biol 15:271–280.

Anton SC. 1993. Internal masticatory muscle architecture in the Japanese macaque and its influence on bony morphology. Am J Phys Anthropol 16(Suppl):50.

Anton SC. 1999. Macaque masseter muscle: internal architecture, fiber length, and cross-sectional area. Int J Primatol 20:441–462.

Anton SC. 2000. Macaque pterygoid muscles: internal architecture, fiber length, and cross-sectional area. Int J Primatol 21:131–156.

Blanksma NG, Vaneijden T. 1995. Electromyographic heterogeneity in the human temporalis and masseter muscles during static biting, open close excursions, and chewing. J Dent Res 74:1318–1327.

Clark RW, Luschel ES, Hoffman DS. 1978. Recruitment order, contractile characteristics, and firing patterns of motor units in the temporalis muscle in monkeys. Exp Neurol 61:31–52.

Dechow PC, Carlson D. 1990. Occlusal force and cramiofacial biomechanics during growth in rhesus monkeys. Am J Phys Anthropol 83:219–237.

Faulkner JA, McCully KK, Carlson D, McNamara JA Jr. 1982. Contractile properties of the muscles of mastication of rhesus monkeys (*Macaca mulatta*) following increase in mucle length. Arch Oral Biol 27:841–845.

Goldberg LJ, Derfler B. 1977. Relationship among recruitment order, spike amplitude, and twitch tension of single motor units in human masseter muscle. J Neurophysiol 40:879–890.

Gower JC. 1966. Some distance properties of latent root and vector methods used in multivariate analysis. Biometrika 53:325–338.

Guelinckx P, Dechow PC, Vanrusselt R, Carlson DS. 1986. Adaptations in the temporalis muscles of rabbits after masseter muscle removal. J Dent Res 65:1294–1299.

Hannam AG, Inkster WC, Scott JD. 1975. Peak electromyographic activity and jaw-closing force in man. J Dent Res 54:694.

Hibbeler RC. 2000. Mechanics of materials, 3rd ed. Upper Saddle River, NJ: Prentice Hall.

Hylander WL. 1979. Mandibular function in *Galago crassicaudatus* and *Macaca fascicularis*: an in vivo approach to stress analysis of the mandible. J Morphol 159:253–296.

Hylander WL. 1986. In vivo bone strain as an indicator of masticatory bite force in *Macaca fascicularis*. Arch Oral Biol 31:149–157.

Hylander WL, Johnson KR, Crompton AW. 1987. Loading patterns and jaw movements during mastication in *Macaca fascicularis*: a bone-strain, electromyographic, and cineradiographic analysis. Am J Phys Anthropol 72:287–314.

Hylander WL, Johnson KR. 1989. The relationship between masseter force and masseter electromyogram during mastication in the monkey *Macaca fascicularis*. Arch Oral Biol 34:713–722.

Hylander WL, Picq PG, Johnson KR. 1991. Masticatory-stress hypotheses and the supraorbital region of primates. Am J Phys Anthropol 86:1–36.

Hylander WL, Johnson KR. 1993. Modeling relative masseter force from surface electromyograms during mastication in non-human primates. Arch Oral Biol 38:233–240.

Hylander WL, Johnson KR. 1997. In vivo bone strain patterns in the craniofacial region of primates. In: McNeill C, editor. Science and practice of occlusion. Chicago: Quintessence Publishing. p 165–178.

Hylander WL, Ravosa MJ, Ross CF, Johnson KR. 1998. Mandibular corpus strain in primates: further evidence for a functional link between symphyseal fusion and jaw-adductor muscle force. Am J Phys Anthropol 107:257–271.

Hylander WL, Ravosa MJ, Ross CF, Wall CE, Johnson KR. 2000. Symphyseal fusion and jaw-adductor muscle force: an EMG study. Am J Phys Anthropol 112:469–492.

Hylander WL, Ravosa MJ, Ross CF. 2004. Jaw muscle recruitment patterns during mastication in anthropoids and prosimians. In: Anapol F, German RZ, Jablonski NG, editors. Shaping primate evolution. Cambridge: Cambridge University Press. p 229–257.

Inman VT, Ralston HJ, Saunders JB, Feinstein B, Wright EW Jr. 1952. Relation of human electromyogram to muscular tension. Electroenceph Clin Neurophysiol 4:187–194.

Kwa SH, Weijs WA, Juch PJ. 1995. Contraction characteristics and myosin heavy chain composition of rabbit masseter motor units. J Neurophysiol 73:538–549.

Lindauer SJ, Gay T, Rendell J. 1993. Effect of jaw opening on masticatory muscle EMG-force characteristics. J Dent Res 72:51–55.

Loeb GE, Gans C. 1986. Electromyography for experimentalists. Chicago: University of Chicago Press.

MacKenna BR, Turker K. 1978. Twitch tension in the jaw muscles of the cat at various degrees of mouth opening. Arch Oral Biol 23:917–920.

Mao J, Osborn JW. 1994. Direction of a bite force determines the pattern of activity in jaw-closing muscles. J Dent Res 73:1112–1120.

Muhl ZF, Grimm AF, Glick PL. 1978. Physiologic and histologic measurements of the rabbit digastric muscle. Arch Oral Biol 23:1051–1059.

Ottenhof FA, van der Bilt A, van der Glas HW, Bosman F. 1993. Control of human jaw elevator muscle activity during simulated chewing with varying bolus sizes. Exp Brain Res 96:501–512.

Ottenhoff FA, van der Bilt A, van der Glas HW, Bosman F, Abbink JH. 1996. The relationship between jaw elevator muscle surface electromyogram and simulated food resistance during dynamic condition in humans. J Oral Rehabilit 23:270–279.

Peyron M, Lassauzay C, AW. 2002. Effects of increased hardness on jaw movement and muscle activity during chewing of visco-elastic model foods. Exp Brain Res 142:41–51.

Proeschel PA, Morneburg T. 2002. Task-dependence of activity/bite-force relations and its impact on estimation of chewing force from EMG. J Dent Res 81:464–468.

Pruim GJ, Tenbosch JJ, Dejongh HJ. 1978. Jaw muscle EMG-activity and static loading of mandible. J Biomech 11:389–395.

Pruim GJ, Dejongh HJ, Tenbosch JJ. 1980. Forces acting on the mandible during bilateral static bite at different bite force levels. J Biomech 13:755–763.

Ralston HJ. 1961. Uses and limitations of electromyography in the quantitative study of skeletal muscle function. Am J Orthodont 47:521–530.

Ross CF. 1995. Muscular and osseous anatomy of the primate anterior temporal fossa and the functions of the postorbital septum. Am J Phys Anthropol 98:275–306.

Ross CF. 2001. In vivo function of the craniofacial haft: the interorbital "pillar." Am J Phys Anthropol 116:108–139.

Ross CF, Patel BA. 2003. Temporal relationship of EMG and muscle force in the anterior temporalis muscle and its utility for finite-element modeling. Am J Phys Anthropol 120(Suppl):180.

Schumacher GH. 1961. Funktionelle Morphologie der Kaumuskulatur. Jena: Gustav Fischer Verlag.

Stern JT Jr, Wells JP, Vangor AK, Fleagle JG. 1976. Electromyography of some muscles of the upper limb in *Ateles* and *Lagothrix*. Yearbook Phys Anthropol 20:498–507.

Strait D, Richmond B, Ross C, Spencer M. 2002. Finite element analysis of a macaque skull: applications for functional morphology. Am J Phys Anthropol Suppl 34:149.

Strait DS, Wang O, Dechow PC, Ross CF, Richmond BG, Spencer MA, Patel BA. 2005. Modeling elastic properties in finite-element analysis: How much precision is needed to produce an accurate model? Anat Rec 283A:275–287.

Tamari JW, Tomey GF, Ibrahim MZM, Baraka A, Jabbur SJ, Bahuth N. 1973. Correlative study of the physiologic and morphologic characteristics of the temporal and masseter muscles of the cat. J Dent Res 52:538–543.

Taylor A, Cody FWJ, Bosley MA. 1973. Histochemical and mechanical properties of the jaw muscles of the cat. Exp Neurol 38:99–109.

Thexton AJ, Hiiemae KM. 1975. The twitch-contraction characteristics of oppossum jaw musculature. Arch Oral Biol 20:743–748.

Weijs WA. 1980. Biomechanical models and the analysis of form: a study of the mammalian masticatory apparatus. Am Zool 20:707–719.

Weijs W, Van Ruijven L. 1990. Models of masticatory mechanics: their reliability, resolving power and usefulness in functional morphology. Netherlands J Zool 40:136–152.

Woittiez RD, Huijing PA, Rozendal RH. 1984. Twitch characteristics in relation to muscle architecture and actual muscle length. Pflugers Arch 401:374–379.